Experiments with photorefractive crystals for holographic interferometry

Robert Magnusson, MEMBER SPIE
Xuqun Wang*
Ali Hafiz
University of Texas at Arlington
Department of Electrical Engineering
Arlington, Texas 76019

Truman D. Black
Lucio N. Tello†
University of Texas at Arlington
Department of Physics
Arlington, Texas 76019

A. Haji-Sheikh
Snezana Konecni
University of Texas at Arlington
Department of Mechanical and Aerospace Engineering
Arlington, Texas 76019

Donald R. Wilson
University of Texas at Arlington
Department of Mechanical and Aerospace Engineering
Arlington, Texas 76019

Abstract. Photorefractive crystals such as iron-doped lithium niobate are versatile recording materials for holographic interferometry. These crystals are self-developing, erasable, and reusable, amply sensitive in the visible region, and possess large information storage capacity, making them attractive for routine interferometry applications. This paper summarizes a variety of experiments in interferometry using iron-doped and undoped lithium niobate crystals for recording the holograms. Double-exposure holography with an argon laser is applied to visualize aerodynamic flow fields, heat transfer patterns, and acoustic waves. A pulsed Nd:YAG laser is used to visualize the details of turbulent aerodynamic fields. Finally, several heat transfer patterns are visualized by holographic subtraction interferometry and real-time interferometry.

Subject terms: interferometry; holography; photorefractive materials.

Optical Engineering 33(2), 596–607 (February 1994).

1 Introduction

Photorefractive materials are of interest for a variety of potential applications, including volume holographic storage for high-capacity optical memories, real-time information processing, real-time holography, holographic interferometry, coherent light amplification, integrated optics, and adaptive optics.[1,2] During the past 20 years, a considerable amount of research work has been performed on these materials. Holographic recording in photorefractive media began in 1968 with work by Chen, LaMacchia, and Fraser.[3] They discovered that laser-induced "optical damage" could be used to record thick phase holograms. Due to additional contributions by many other researchers, these crystals now constitute an important class of optical storage materials.

Holographic interferometry is important for many diagnostic applications, such as aerodynamics, heat and mass transfer, stress analysis, and plasma dynamics.[4] It yields global visualization of refractive-index distributions with quantitative results without affecting the phenomena under study. The principle of holographic interferometry can be described as any method involving the comparison of two or more light waves by holographically reconstructing at least one of them.[5] Many variations on this general theme exist, such as real-time holographic interferometry, double-exposure holographic interferometry, time-average holographic interferometry, and short-pulse holographic interferometry. By holographically storing a reference wavefront, the interference of two waves passing through an object at two different times can be obtained. Furthermore, double-exposure holograms can be recorded and stored for different angular views through the object leading to multidirectional interferometry and true 3-D visualization by tomographic techniques. Interest is high regarding the use of short-pulse holographic interferometry to characterize high-speed transient flow phenomena. The optical components and test windows need not be of exceptionally high quality because any constant distortions of the wavefronts caused by the optics are compensated[5]; thus, the interference pattern depends only on the phase variation between the first and second exposures. Short-pulse holographic interferometry offers an advantage over cw holographic interferometry by not requiring vibration isolation.

The recording medium in most of the holographic interferometry experiments reported to date has been film, which

* Current affiliation: Spectra Diode Labs, San Jose, California.
† Current affiliation: Computalog Research Inc., Fort Worth, Texas.

Paper 16112 received Nov. 14, 1992; revised manuscript received May 7, 1993; accepted for publication May 8, 1993. This paper is a revision of a paper presented at the SPIE conference on Holographics International '92, July 1992, London, England. The paper presented there appears (unrefereed) in SPIE Proceedings Vol. 1732.
© 1994 Society of Photo-Optical Instrumentation Engineers. 0091-3286/94/$6.00.

yields good results when relatively few exposures are to be recorded or a steady-state phenomenon is under study. Whereas photographic film is several orders of magnitude more sensitive than the crystals used for the experiments reported in this paper (typical exposure ~ 1 J/cm^2), the use of film may be more difficult due to the large number and speed of needed exposures, mechanical film movement, the tedium of development, and other problems, especially in time-varying flow visualization experiments. For many applications utilizing holographic interferometry, photorefractive materials may be the optimum recording media, which can be argued as follows:

1. The holograms form rapidly by charge migration[6] and the electro-optic effect, with no chemical development needed.
2. The inherent large information storage capacity (theoretically 10^{12} bits/cm^3) can be utilized by angular or wavelength multiplexing.
3. The crystals are erasable and reusable without fatigue.
4. The holograms can be fixed in some photorefractive materials by thermal, electrical, or optical treatments.
5. The materials possess a wide range of hologram lifetimes: from years or months to less than a microsecond.
6. Real-time recording and readout is possible.
7. Short-pulse recording of high-speed phenomena is possible.
8. The materials have ample sensitivity and good resolution.
9. Due to the variety of photorefractive materials available, the recording media and their attendant properties can be selected to suit a particular application.
10. The crystals are mainly sensitive to the recording laser light so that the work can take place with reasonable ambient light levels.

The photorefractive effect has been observed in numerous media.[2,7] For the experiments reported in this paper, lithium niobate has been selected as the storage material because it possesses the required long hologram lifetimes needed for the chosen applications. In $LiNbO_3$, the basic process of hologram formation can be generally described as follows[7]: With the crystal placed at the intersection of two interfering laser beams, electrons are excited from traps within the bright fringes of the interference pattern. These electrons then migrate out of the bright fringes and are retrapped in the dark fringes. The resulting spatially varying charge distribution creates space-charge fields that modulate the refractive index of the crystal through the electro-optic effect. This spatially varying refractive index constitutes the stored hologram grating.

In this paper, several experiments in holographic interferometry that used undoped and iron-doped lithium niobate crystals for recording the holograms are described. These include double-exposure holographic interferometry with cw and pulsed lasers, holographic subtraction interferometry, and real-time interferometry with photorefractive reference holograms. Example applications such as visualization of aerodynamic flow fields, heat transfer patterns, and acoustic fields are presented.

2 Double-Exposure Holographic Interferometry

2.1 *Background*

In double-exposure holographic interferometry, a hologram of the object in an arbitrary state at an instant of time is first recorded in the crystal. A second hologram of the object in another state at another instant of time is then recorded on top of the first one by means of the same reference beam. Retrieval of the information is achieved by blocking the object beam and reading the double-exposure hologram with the reference beam. This reconstructed wave will travel in the direction of the original object wave. The interference of the two simultaneously reconstructed object waves produces the interferogram that can be viewed on a screen and recorded by a camera. The interferogram will reveal information about the light path variations of the two recordings.

The body of work involving holographic interferometry using photorefractive crystals as the storage medium is relatively small. In particular, very few papers have addressed double-exposure holographic interferometry, which is of prime interest in this section. Magnusson et al.[8] reported initial experimental results in iron-doped lithium niobate (Fe:$LiNbO_3$) using a low-power laser, thus requiring rather long exposures (~1 s). These results were later greatly improved by the use of a high-power argon laser. Experimental results on aerodynamic flow-field visualization[9] and heat-flux evaluation[10] were subsequently reported.

2.2 *Experiments with a Continuous-Wave Laser*

The holographic interferometer is shown in Fig. 1. The variable beamsplitter divides the beam of a high-power cw argon-ion laser (wavelength $\lambda = 514.5$ nm) into two beams. The object beam travels through a spatial filter and is then collimated by a separate lens into a plane wave with a diameter of 50 mm. The object is placed at a distance 30 cm in front of the Fourier transform lens. The reference beam passes through a focusing lens to adjust the spot size and to control the input power density. The reference and object beams intersect in the crystal that is located 10 mm away from the back focal plane of the Fourier transform lens. This out-of-focus approach is used to avoid saturation of the material due to the high power densities that arise exactly in the focal plane. The angle between the reference beam and the object beam is 30 deg. Relatively large crystal transverse dimensions (10×10 mm^2) permit recording at various locations because of the small volume of the overlapping beams. This implies a large data storage capacity when employing the angular multiplexing technique. In the current experiments, the reference and object beams have approximately 4 and 3 mm^2 spot areas, respectively. The iron-doped lithium niobate crystals used in these experiments are y-cut and are used in the transmission geometry configuration. The thickness of the 0.05 mol% iron-doped crystal is 2 mm; the undoped one is 1 mm thick. It is important that the crystal optic axis be oriented orthogonal to the holographic fringes to take advantage of the photovoltaic effect[7] and the attendant efficient charge transport. The two beams are *s*-polarized (electric field vector normal to the plane of incidence) when

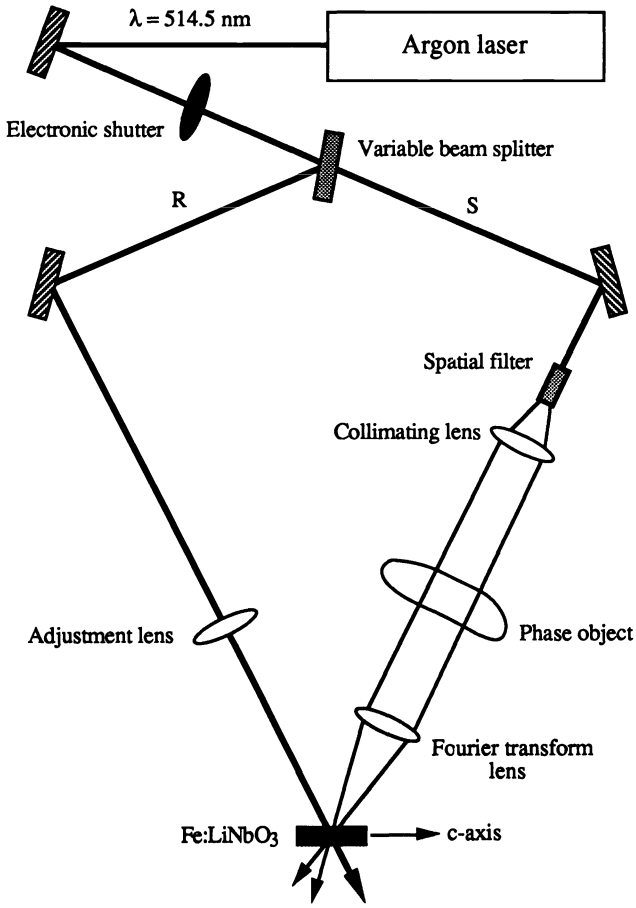

Fig. 1 Continuous-wave holographic interferometer. The phase object can be any transparent medium of interest.

recording the holograms. Typically, the total recording power density used in these experiments is ~15 to 30 W/cm^2 for the two beams combined with exposure times of ~10 to 100 ms. The reference (R) to object (S) beam ratio is between 3 and 4. The refractive-index distributions that are visualized in the interferograms produced are generated by a small-scale wind tunnel, an electronic chip, or an acoustic transducer in a water tank.

The wind tunnel has a window (~15×30 mm^2) with glass plates to allow transmission of the object plane wave. Within the window inside the tunnel, objects with various aerodynamically interesting shapes can be mounted to generate the flow fields. In these experiments, the wind tunnel is driven by nitrogen gas from a high-pressure compressed nitrogen gas cylinder. To change the physical conditions of the flow, the tunnel has three adjustments: throat height, pitch angle, and diffuser opening. When the throat height is decreased the Mach number is increased but the pressure is decreased and vice versa. The pitch angle changes the angle of the aerodynamic shock waves observed in these experiments. The diffuser setting is intended to vary the velocity of the flow. Thus, the experimental conditions can be set as required through these adjustments.

The electronic chip, of dimensions $21.5 \times 6.4 \times 2$ mm^3, is heated by an applied voltage. The temperature is monitored by a thermocouple mounted to the bottom surface of the chip. The chip is enclosed in a glass housing to prevent unwanted air currents from disturbing the temperature distribution. The thermally induced refractive-index spatial distributions are visualized in air and in deionized water.

The ultrasonic transducers consist of PZT-4 disks (25.4 mm in diameter) with full silver electrodes on both sides. To eliminate any signals or reflections from the back acoustic port, an air backing assembly is attached. To obtain an interferogram, the transducers are placed in a water tank. Then two exposures are taken; the first with no acoustic field and the second with the acoustic field turned on. The transducer transmits an acoustic wave against a glass wall. The resulting standing waves generated are visualized in the volume of water intercepted by the expanded laser beam. All the transducers are operated with an adjustable-amplitude sinusoidal signal at the resonant frequency of their fundamental longitudinal thickness mode.

In this research, sequences of aerodynamic flow fields for a range of objects of various sizes and shapes have been recorded. Typically, the first double-exposure hologram is recorded under symmetric conditions (unslanted holograms) whereas the rest are written by angular multiplexing with ~0.1- to 1-deg angular spacing (achieved by computer-controlled crystal rotation) between the holograms. Example aerodynamic interferograms produced by the reconstruction of two double-exposure hologams (first exposure, flow off; second exposure, flow on) are shown in Figs. 2 and 3. The object in Fig. 2 is an ordinary cylinder with a hole on the tip and an extended slit along its side. The diameter increases gradually in two regions. The object in Fig. 3 has the shape of a hammer head. These results demonstrate the visualization of the aerodynamic flow field created by these objects. The shock waves generated by the tips and bouncing off the tunnel walls are clearly shown.

If a Mach 1 flow is assumed (the speed of the flow is then equal to the speed of sound, ~341 m/s) in Figs. 2 and 3, an air molecule needs ~88 μs of transit time to travel along the 30-mm-long wind tunnel test section. The 30-ms flow-on exposure corresponds to approximately 340 transit times of the air stream; thus, these cw visualizations show an average of the flow during a time span exceeding 300 such transit times. Note that the tips of the objects are different, accounting for the difference in the shapes of the bow waves. A

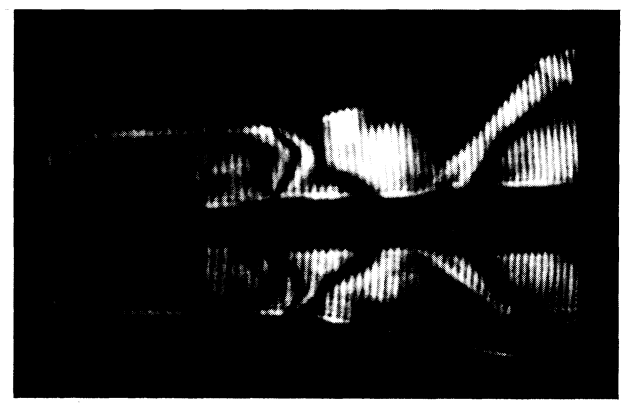

Fig. 2 Interferogram produced by the reconstruction of two double-exposure holograms. The aerodynamic test object is a cylinder with a hole on the tip and an extended slit along its side. The diameter increases gradually in two regions. The vertical fine-line pattern is due to multiple internal reflections in the crystal.

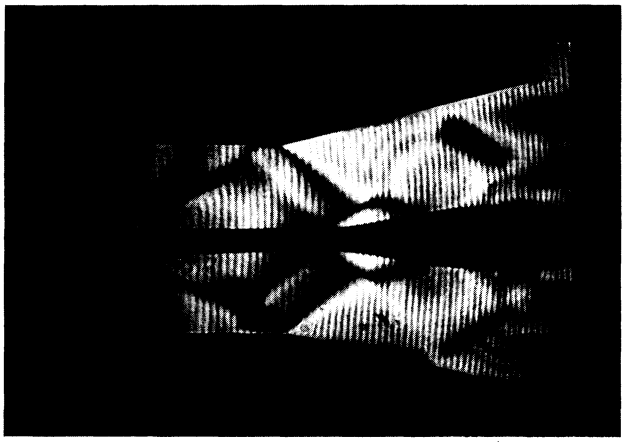

Fig. 3 Interferogram produced by the reconstruction of two double-exposure holograms. The aerodynamic test object has the shape of a hammer head.

variety of test objects have been used for this work under widely varying experimental conditions. The results are easily and conveniently obtained.

To further quantify the storage of multiple double-exposure holograms via angular multiplexing, several sets of interferograms have been produced with the diffraction efficiency and angular selectivity of each such double-exposure hologram measured. A curve of the diffraction efficiency versus the external readout angle is presented in Fig. 4. In this collection of holograms, multiplexing occurs at 0.25 deg intervals. All the interferograms are recorded under the same conditions. Typical diffraction efficiency for *s*-polarization readout is seen in this figure to be 0.15% to 0.25%. The sidelobe structure is sketched by means of the analytical expression for diffraction efficiency from Kogelnik's theory[11] matching the theory and experiments at each Bragg angle only. This gives an indication of the angular spread of the holograms in practice.

In Fig. 5, it is indeed verified that the theory gives a reasonable estimate of the angular behavior. There, the angular selectivity of a single double-exposure hologram with a Bragg angle of $\theta' = 15.5$ deg is examined more carefully. Theory[11] and experiment are compared matching the two at the Bragg angle only. The theory intended for infinite plane-wave readout of thick hologram gratings is seen to describe adequately the much more complicated situation of two superimposed Fourier transform data holograms, at least for the experimental conditions used here.

The object waves in Figs. 2 and 3 traverse what are actually 3-D flow fields. Figure 6 shows flow-field visualization in which the object used (a wedge) is constant along the laser beam propagation direction (i.e., spans across the wind tunnel), thus appearing more like a 2-D structure. The use of objects that generate 2-D flow facilitates interferogram interpretation and data analysis.

For heat-flux evaluation, the object selected is an electronic chip, heated by applying a voltage to it. The double-exposure hologram is formed by recording a background hologram with the voltage off and superimposing on top of it another hologram with the applied voltage turned on. Example results are given in Figs. 7 and 8.

Finally, experimental results illustrating acoustic wave fields in a water tank are presented in Figs. 9, 10, and 11. Useful information regarding the spatial power distribution of the ultrasonic waves is obtained and an experimental determination of their wavelengths is made. The wavelengths measured agree well with the formula $\lambda_a = v_a / f_a$ where v_a is the acoustic velocity in water ($\sim$1.5 km/s) and f_a is the frequency.

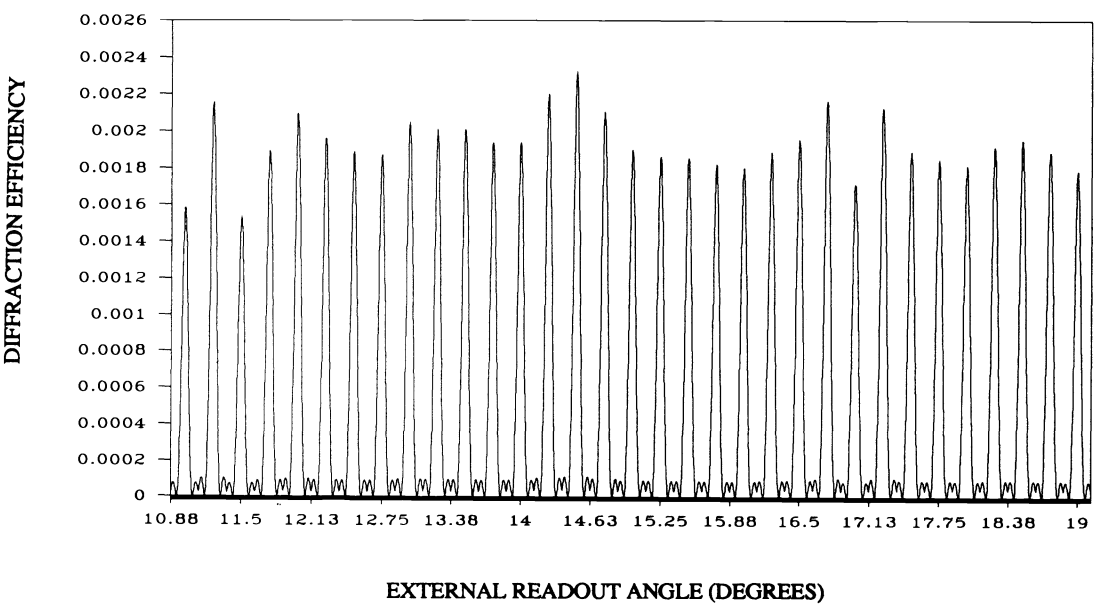

Fig. 4 Angularly multiplexed double-exposure holograms. The diffraction efficiency versus the external readout angle is shown. Thirty-three double-exposure holograms are recorded at 0.25-deg angular separation intervals. The curves are generated using Kogelnik's theory matching the theory and experiments at the Bragg angle only.

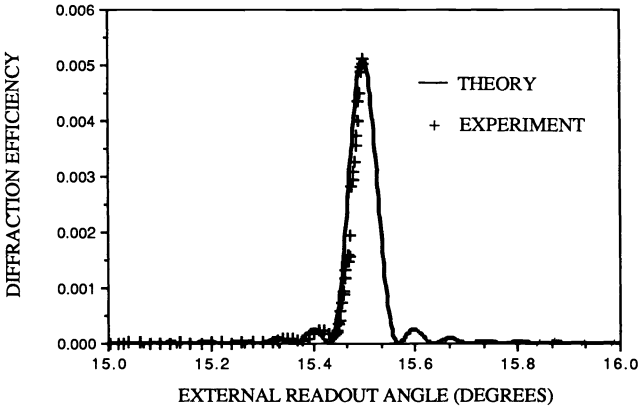

Fig. 5 Angular selectivity of a double-exposure hologram. Theory and experiment are matched at the Bragg angle (15.5 deg) only. The theoretical plot is generated by means of Kogelnik's theory.

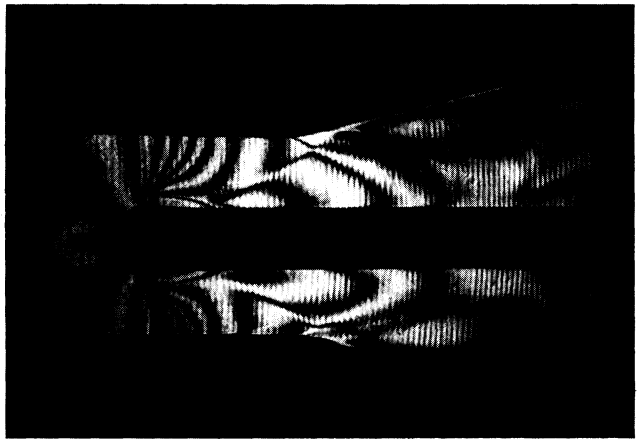

Fig. 6 Interferogram of a 2-D flow field in the wind tunnel. The aerodynamic test object is a wedge spanning the tunnel in the direction of the object wave in the middle of the window.

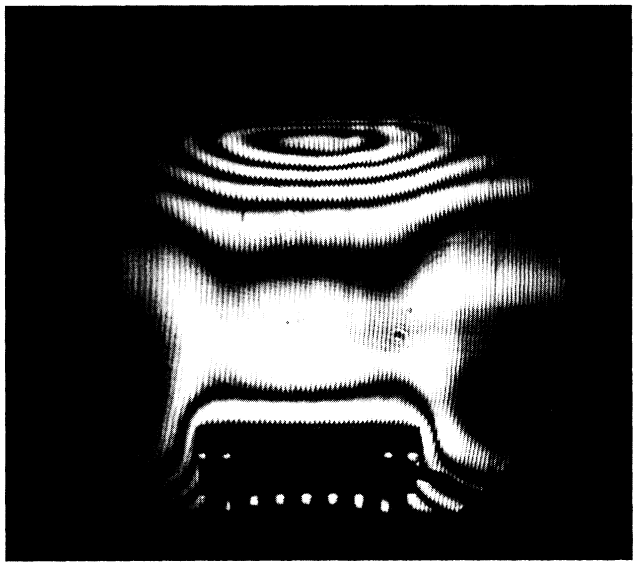

Fig. 7 Interferogram corresponding to heat-flux visualization. The object is an electronic chip mounted longitudinally. The temperature of the chip surface is 225°C as measured by a thermocouple.

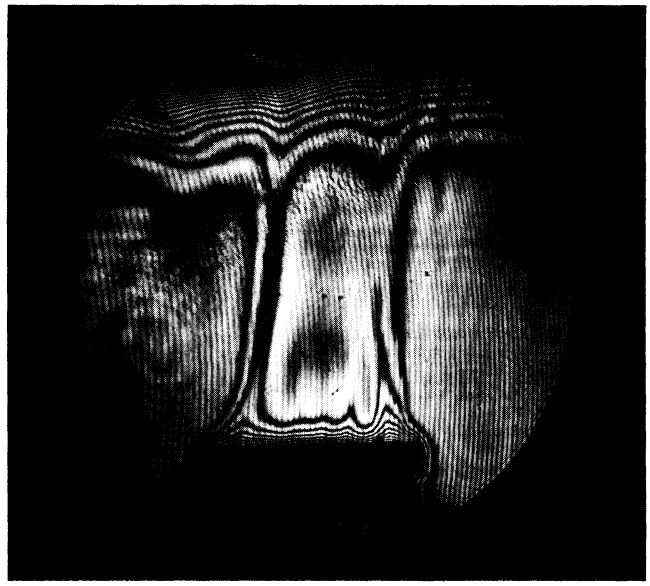

Fig. 8 Interferogram corresponding to heat-flux visualization. The object is the same as in Fig. 7 but the chip is in deionized water. The temperature of the chip is 32.5°C.

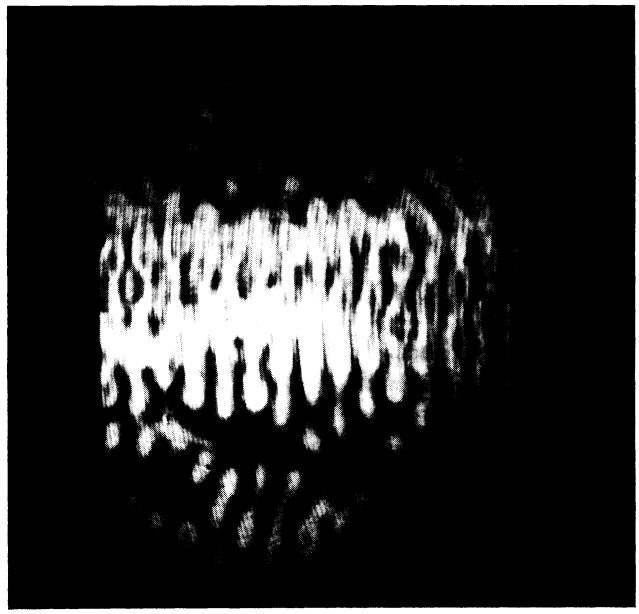

Fig. 9 Visualization of a standing acoustic wave in a water tank. The acoustic frequency is 250 kHz and the wavelength is experimentally found to be 6.1 mm.

2.3 *Experiments with a Pulsed Laser*

The high-power pulsed-laser holographic interferometry recording system is shown in Fig. 12. The laser used is a Q-switched, frequency-doubled Nd:YAG laser with a pulse length of 5 ns. The fundamental wavelength is $\lambda = 1064$ nm. The laser is specified at 1200 mJ of energy per pulse at this wavelength. The angle between the recording beams is 30 deg. Typical writing power density is 50 MW/cm^2 for recording at $\lambda = 532$ nm with additional 50 MW/cm^2 at $\lambda = 1064$ nm for recording with infrared enhancement. The

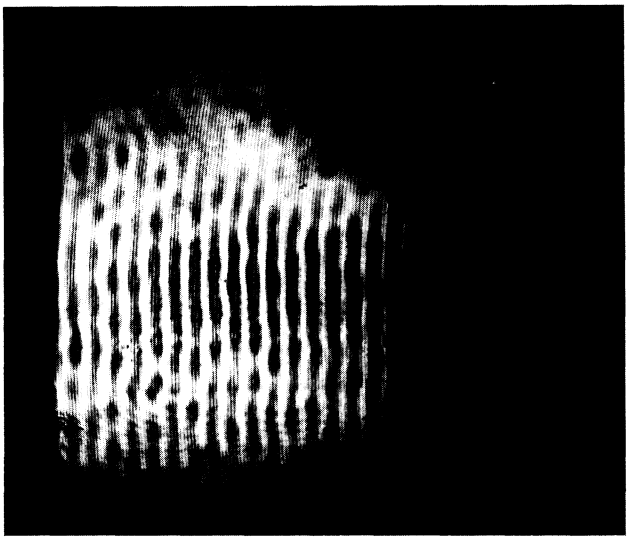

Fig. 10 Visualization of a standing acoustic wave in a water tank. The acoustic frequency is 450 kHz and the wavelength is experimentally found to be 3.3 mm.

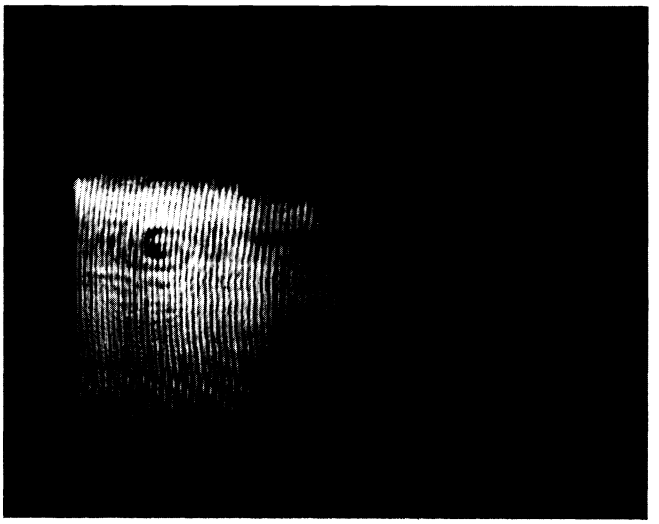

Fig. 11 Visualization of a standing acoustic wave in a water tank. The acoustic frequency is 1000 kHz and the wavelength is experimentally found to be 1.1 mm.

spot sizes of the reference, object, and infrared beams on the crystal are approximately 7, 5, and 15 mm^2, respectively. Crystals of undoped (1 mm thick) and 0.05 mol% iron-doped (2 mm thick) $LiNbO_3$ were used in the pulsed recording experiments.

As shown in Fig. 12, the recording wavelength is 532 nm; the beam is emitted from port 1 and split by a beamsplitter.

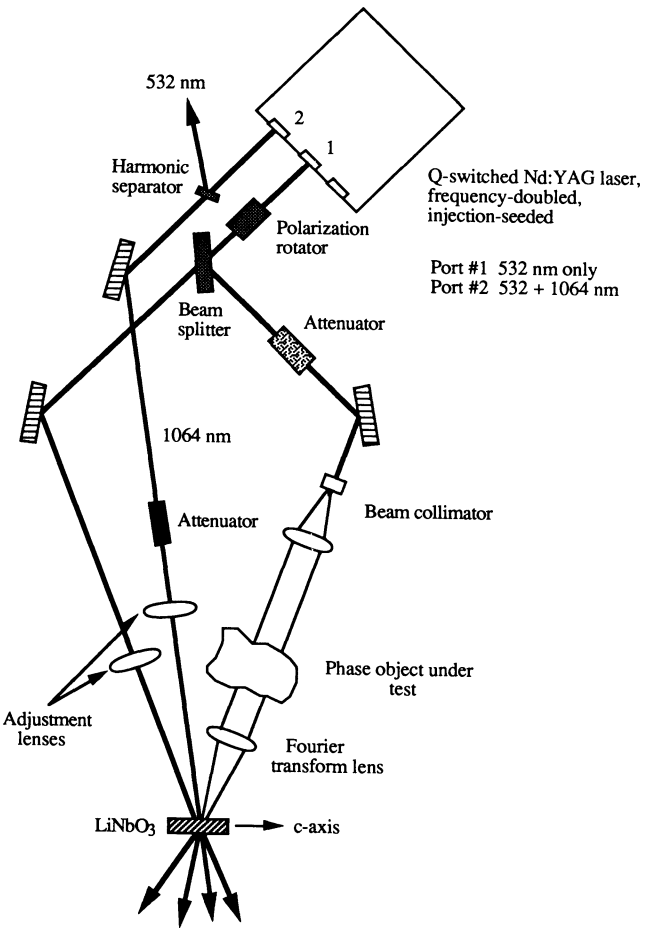

Fig. 12 High-power pulsed-laser holographic interferometer.

The polarization is rotated to *s*-polarization by a polarization rotator. The object beam passes through an attenuator to adjust the power incident on the crystal and to vary the beam ratio. Collimation into a beam with a 100-mm diameter is achieved by a system of diverging and converging lenses. The beam traverses the object that is placed approximately one focal length in front of a Fourier transform lens. The reference beam is adjusted by a lens and then interferes in the crystal with the object beam. The point where the beams meet is about 10 mm away from the focal plane of the transform lens (i.e., out-of-focus Fourier transform approach).

For recording with IR enhancement, the beam from port 2 is harmonically separated (i.e., the radiation with $\lambda = 532$ nm is dumped) and the infrared beam is transmitted through an attenuator and an adjustment lens. Then, the beam impinges on the spot in the crystal at which the two green beams are present simultaneously (see Fig. 12).

The procedure for recording the double-exposure hologram is basically the same as before except that the recording pulses are 5 ns each. Single-wavelength recording is accomplished by the frequency-doubled (green) beams alone. The interferogram is retrieved by blocking the object beam and reconstructing with the reference beam. Recording with IR enhancement is similar except that in addition to the two green beams, the infrared beam is also present. The wind tunnel is the only object used in this experimental procedure.

In Fig. 13, a single-wavelength (i.e., $\lambda = 532$ nm only used) double-exposure hologram is shown. This demonstrates flow-field visualization when a pulsed laser is used. The object is shaped like the hammer head shown previously in Fig. 3. Note that the turbulence present around the object can now be seen. A result obtained by the IR-enhancement ($\lambda = 532$ nm, $\lambda = 1064$ nm simultaneously applied) recording technique is demonstrated in Fig. 14. The object has a circularly symmetric ball tip. The sensitivity (i.e., diffraction efficiency per pulse of green light) of the material is increased when an infrared beam is present simultaneously.

Assuming a Mach 1 flow in the previous results, the pulsed-laser visualization represents a virtual instantaneous snap shot (all motion "frozen") of the air wave in each interferogram. As in the cw experiments, an air molecule needs ~88 μs to travel along the window. The exposure pulse length is a negligible fraction (5 ns/88 μs $= 57 \times 10^{-6}$) of the transit time.

All of the previously reported results were recorded in 0.05% iron-doped $LiNbO_3$. Results obtained with undoped $LiNbO_3$ are shown in Fig. 15. The object (used in Fig. 6 also) is an arrow-shaped wedge that produces a 2-D flow field in the window of the tunnel. The diffraction efficiency is low, about 0.05%. The double-exposure hologram in Fig. 15 is recorded by means of the single-wavelength holographic technique.

To quantify further the difference between recording with green light only and an IR-enhanced recording, a curve of the diffraction efficiency versus multiplexing angle (i.e., the angle that the crystal is rotated between exposures) for single-exposure, single-pulse, plane-wave holograms (no object) is presented in Fig. 16. The crystal used is undoped $LiNbO_3$. The system in Fig. 12 is used, but the object beam is not collimated and travels directly to the crystal (i.e., record with raw laser beams). The reference and object beams have the same spot areas (~5 mm^2) and the beam ratio $R/S = 1$. The infrared beam has a spot area of ~10 mm^2. Superposition of holograms by angular multiplexing is used. In Fig. 16, seven holograms with the same energy in each 5-ns pulse are re-

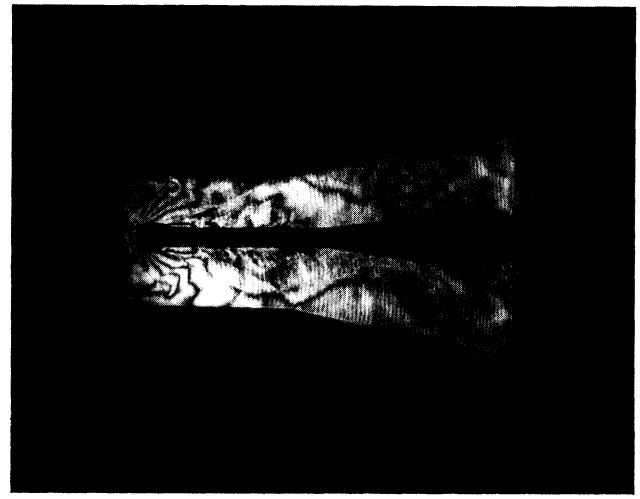

Fig. 14 IR-enhanced recording of flow field inside the window test area. The object is a circularly symmetric rod with a ball tip.

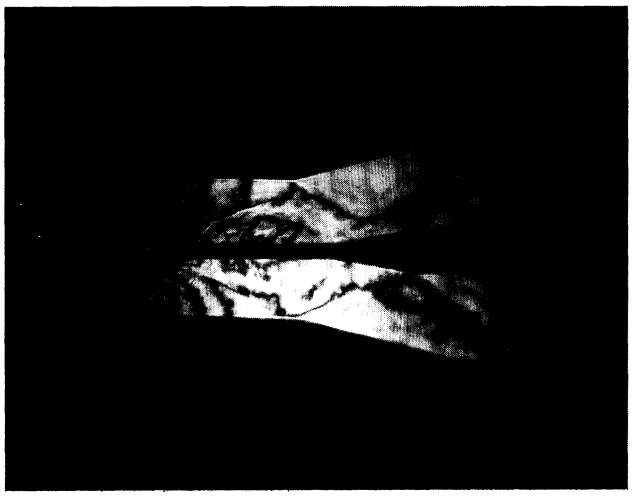

Fig. 13 Demonstration of flow-field visualization using pulsed recording. The object has the shape of a hammer head; compare with Fig. 3.

Fig. 15 Pulsed 2-D flow-field visualization in undoped lithium niobate. The object is the same as in Fig. 6.

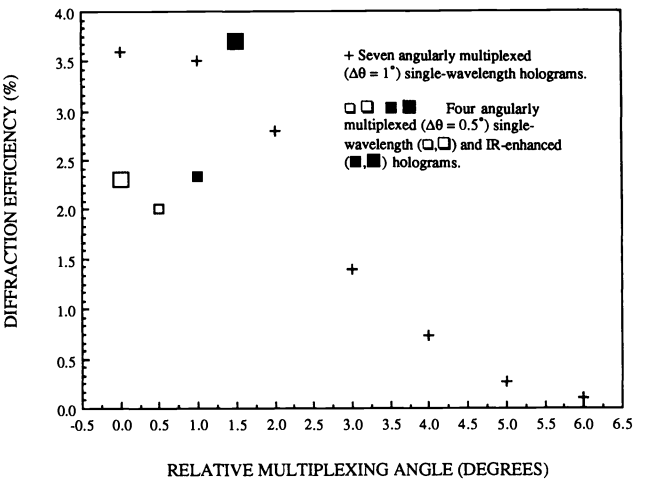

Fig. 16 Angular multiplexing of holograms in undoped $LiNbO_3$. The power density used for green light recording is 50 MW/cm^2. The power densities for IR-enhanced recording are 50 MW/cm^2 (green), 50 MW/cm^2 (infrared at 1 deg), and 100 MW/cm^2 (infrared at 1.5 deg).

corded at the same location in the crystal at 1-deg angular separation intervals. The diffraction efficiency starts off at maximum value and degrades as more holograms are superimposed at different angles. Therefore, saturation of the dynamic range of this undoped crystal by means of green light recording is observed. In another crystal spot, four holograms are recorded. The first two holograms (at 0 and 0.5 deg) are recorded with $\lambda = 532$ nm for which the angular separation is 0.5 deg (diffraction efficiencies: $\eta_1 = 2.3\%$ and $\eta_2 = 2.0\%$). Then at 1 and 1.5 deg two IR-enhanced holograms were recorded. The first (50 MW/cm^2 infrared power density) has a 2.4% diffraction efficiency, while the second obtains a 3.7% diffraction efficiency when stronger infrared illumination (100 MW/cm^2 power density) is used. Material saturation is therefore counteracted by addition of the IR beam.

The absorption mechanisms operative during hologram recording in photorefractive crystals have been discussed by von der Linde and Glass,[12] by Glass,[7] and by Wood et al.[13] Using green light only at the power density levels ($\sim$50 MW/cm^2) applied in the current work, it is possible that two-photon absorption[7,12] (virtual state process) is occurring in both the doped and undoped $LiNbO_3$ crystals. The IR beam enhancement observed could be due to excitation of shallow traps or to two-step absorption via a real intermediate state.[7,12,13]

3 Holographic Subtraction Interferometry

3.1 *Background*

In 1965, Gabor et al.[14] showed that optical image subtraction can be accomplished holographically by introducing a π phase shift in the reference beam between the two exposures. Their holograms were recorded on photographic plates. Ten years later, Huignard, Herriau, and Micheron[15] employed this technique to implement coherent subtraction of images by means of photorefractive crystals. The procedure is first to record a Fourier transform hologram of a given scene in a photorefractive crystal and then record a superimposed Fourier transform with similar amplitude of another scene but with a phase shift of π in the reference beam. The result is the production of a refractive-index grating complementary to the grating constituting the first hologram. Reconstruction reveals that parts common to both scenes have been erased. On binary data, this corresponds to the EXCLUSIVE OR logic operation. Also, it has been demonstrated that any given hologram (or even a specific part of that hologram) in a stack of angularly multiplexed holograms can be selectively erased. This is called *coherent selective erasure.*[15] Using the same basic principle, Trolinger has demonstrated the application of holographic subtraction interferometry.[16] He used a system with two reference beams and applied the phase shift during reconstruction. Guest, Mirsalehi, and Gaylord[17] have successfully employed similar ideas for binary image subtraction or EXCLUSIVE OR processing.[17]

3.2 *Experimental Results*

The experimental arrangement for holographic subtraction interferometry is similar to that in Fig. 1 except that a commercial electro-optic phase modulator is placed in the reference arm. In this experiment, the test object is a short coil that is heated up between the two exposures with a 20-V applied voltage. Two equal exposures are made. The first exposure is with a cold object and the second one after the object has been heated. The reconstruction gives a heat transfer pattern as shown in Fig. 17(a). When a π phase shift is introduced (by the phase modulator) between the two exposures, the background and the parts that are not changed by heating are erased and only differential information is reconstructed as shown in Fig. 17(b).

4 Real-Time Interferometry

4.1 *Background*

Real-time interferometry is commonly implemented by means of a hologram of the object scene in a given reference state. This reference state is continuously reconstructed by the original reference beam and a dynamically perturbed version of the object scene is superimposed by the direct object wave. Thus, in this version of real-time interferometry, only one reference hologram needs to be recorded against which a sequence of object scenes can be interferometrically compared.

Ideally, the reference hologram is recorded and developed *in situ* so that no auxiliary, unwanted fringe patterns are generated by improper placement of the hologram. *In situ* development of photographic emulsions can be accomplished by use of liquid gates.[18] To avoid the problems associated with film development and subsequent accurate placement of the reference hologram, photorefractive materials can be used. This section reports results obtained by real-time interferometry using iron-doped lithium niobate to record the reference holograms. Fe:$LiNbO_3$ allows storage of holograms for an extended period as determined by the level of Fe doping. If low-power laser beams are used, the crystal hologram is erased very slowly. It is found that when the experimental parameters (such as the iron-doping level of the crystal, diffraction efficiency of the reference hologram, beam intensity ratio, and absolute power levels) are properly chosen, the pattern of interference fringes representing the changes of the object can be clearly observed in real time

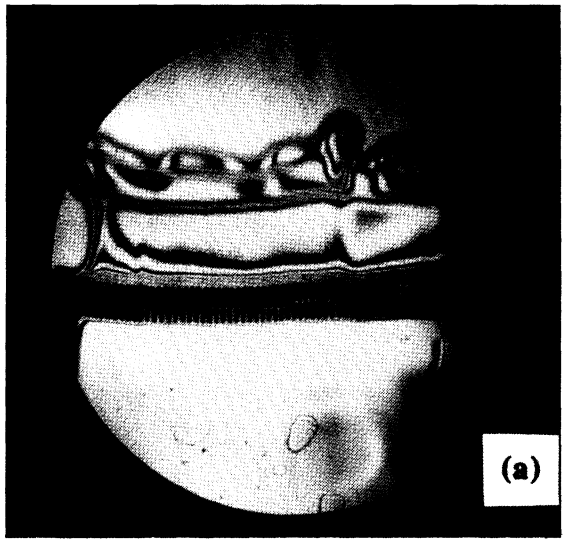

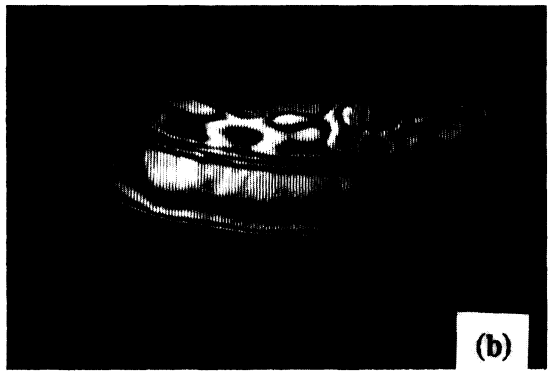

Fig. 17 Holographic subtraction interferometry in Fe:$LiNbO_3$: (a) Without π phase shift between the two exposures and (b) with π phase shift between the two exposures and thus the background is erased. The object is a heated coil.

and that the same reference hologram can be used for a long sequence (several minutes) of input data. This approach can be of great value in practical interferometry where extended physical variations of, for example, refractive-index fields generated by heat, acoustic waves, air currents, or pressure gradients need to be analyzed. High-speed transient phenomena can also be handled by this technique.

Related published papers include those by Huignard and Herriau,[19] Ja,[20] and Guest, Mirsalehi, and Gaylord.[17] Huignard and Herriau[19] used real-time double-exposure interferometry in Bi_{12} SiO_{20} crystals. Due to the short lifetime of the holograms under illumination, their processing time was only 40 ms. Ja[20] applied $Bi_{12}GeO_{20}$ crystals in a four-wave mixing geometry and reported a processing time of 0.8 s. Guest, Mirsalehi, and Gaylord[17] stored digital data pages in a photorefractive crystal that were then reconstructed with the reference beam to implement binary subtraction between the reconstructed image and the directly transmitted image of another data page.

4.2 *Experimental Results*

The experimental arrangement for recording the reference hologram is that of Fig. 1. An argon-ion laser operating at a wavelength of 514.5 nm with 2-W power output is used as the light source to write holograms in iron-doped lithium niobate crystals (size $10 \times 10 \times 2$ mm^3, one with 0.005 mol% iron doping and another one with 0.05 mol% iron doping). The beam is divided into object (S) and reference (R) beams and adjusted so that the power in the reference beam is approximately 10 times that of the object beam. Typical beam power levels (measured at the crystal) are $P_S = 20$ mW and $P_R = 200$ mW. In one sequence of experiments, the object consists of three resistor chips in a glass enclosure. The reference hologram is recorded with the power supply to the chips switched off. For the crystal with 0.005 mol% iron, a reference hologram with 3.3% diffraction efficiency is recorded. All of the parameters except the laser output power should remain fixed throughout the experiment to avoid generating auxiliary fringes.[21]

The experimental setup for real-time interferometry is also that shown in Fig. 1 but with the power supply for the object switched on. To avoid hologram recording during processing, the laser output power is decreased from 2 W to 40 mW. For the lightly doped (0.005%) crystal with a processing time of up to 10 min, negligible hologram recording takes place. The much stronger reference beam reconstructs the stored reference hologram and interference between the reconstructed wave and the direct image wave representing the changing object occurs dynamically. Thus, the variations in the object are monitored by comparing the object continuously with the same background producing a sequence of real-time interferograms of the heat flow emanating from the chips. The temperature of the surface of each chip is measured by thermocouples. As an example, Fig. 18 shows the interferogram of a heat flow pattern after application of voltage to the central chip as it is disturbed by a forced airflow from the left. Figure 19 illustrates the result of applying voltage to all three chips in the absence of forced flow.

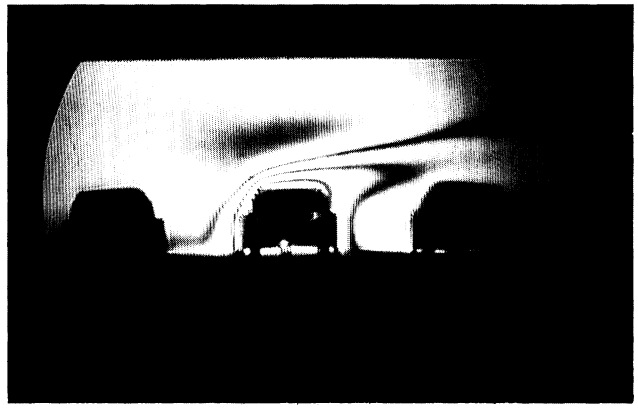

Fig. 18 Real-time interferogram of a heat flow pattern disturbed by airflow from the left. The temperature of the central chip is 158°C. The flow rate is 2.9 l/min.

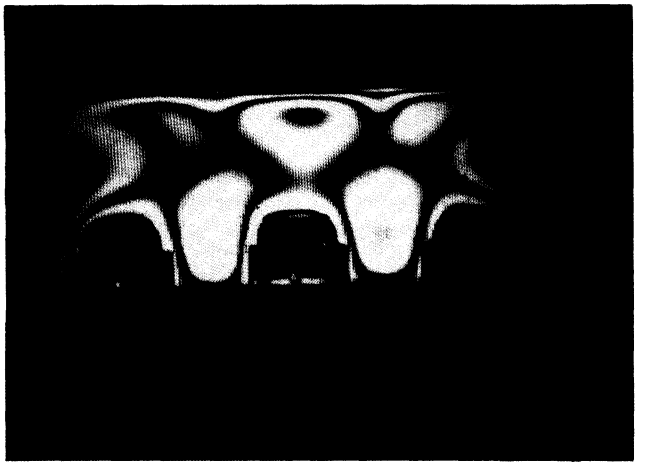

Fig. 19 Real-time interferogram of a heat flow pattern (natural convection) after application of voltage to all three chips. The temperatures of the chips from left to right are 141, 174, and 165°C, respectively.

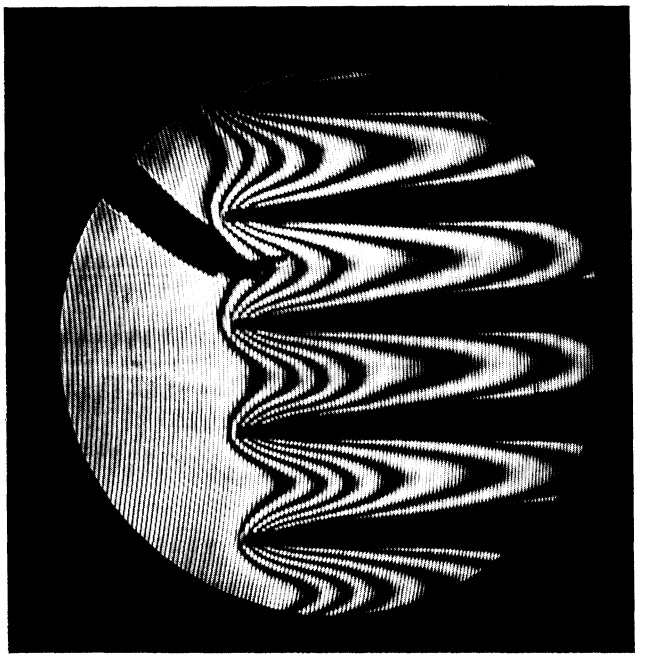

Fig. 20 Real-time interferogram of a heat flow pattern in water around heated fins. The difference in the temperatures of the fins and water is 1°C. (Temperature of the fin is 23°C.)

In another experimental study employing similar procedures, a heat sink assembly comprised of a number of aluminum fins is submerged in a pool of water. The dimensions of the heat sink are $45 \times 105 \times 55$ mm^3. The fin assembly is placed over a heater. Two thermocouples are used to monitor the temperatures, one at the base and one to measure the temperature of the water outside the fin assembly. This latter temperature is useful to check the temperature field determined from the location of the fringes. Constant density lines around the fins are observed as power is applied to the heater. Figure 20 shows the water density pattern for a temperature difference of 1°C. A denser fringe pattern is shown in Fig. 21 for a temperature difference of 3°C.

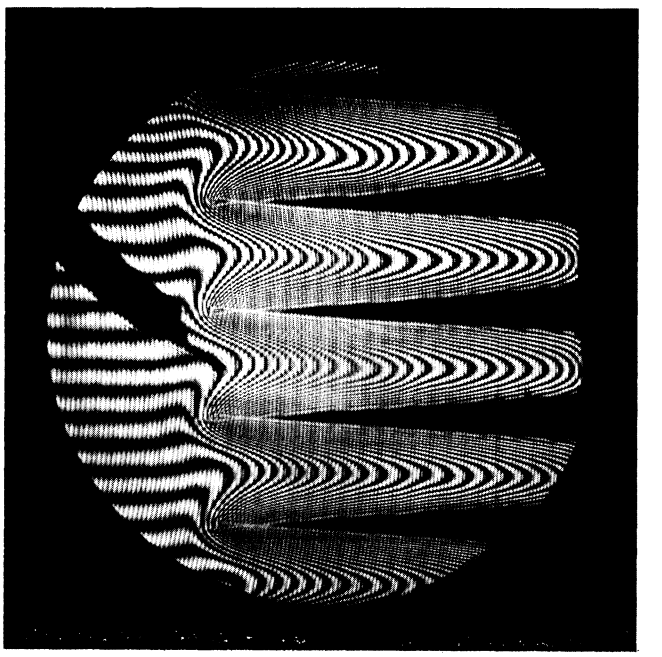

Fig. 21 Real-time interferogram of a heat flow pattern for a submerged heat sink. The temperature difference is 3°C.

5 Conclusions

In this paper, results obtained with photorefractive crystals possessing long hologram decay time constants (near-archival storage) have been presented. This storage medium is found to be useful for double-exposure holographic interferometry with cw and pulsed lasers, holographic subtraction interferometry, and real-time interferometry with photorefractive reference holograms. Clearly, Fourier transform holographic interferometry using photorefractive materials is a viable experimental technique. It is convenient and straightforward in applications such as aerodynamics, acoustics, and heat transfer.

Acknowledgments

Thoughtful comments by one of the reviewers helped improve this paper. This material is based in part on work supported by the Texas Advanced Technology Program under Grants 003656-023 and 003656-045 and by the U.S. Army Research Office under Grant DAAL03-86-K0149. Ali Hafiz would like to acknowledge the support of the Hariri Foundation.

References

1. T. K. Gaylord, "Digital data storage" in *Handbook of Optical Holography*, H. J. Caulfield, Ed., pp. 379–413, Academic Press, New York (1978).
2. P. Günter and J. P. Huignard, Eds., *Photorefractive Materials and Their Applications I*, Springer-Verlag, Berlin (1988).
3. F. S. Chen, J. T. LaMacchia, and D. B. Fraser, "Holographic storage in lithium niobate," *Appl. Phys. Lett.* **13,** 223–225 (1968).
4. C. M. Vest, *Holographic Interferometry*, John Wiley and Sons, New York (1979).

5. A. N. Zaidel, "Application of holographic interferometry for plasma diagnostics," *Sov. Phys. Usp.* **29,** 447–466 (1986).
6. A. M. Glass and J. Strait, "The photorefractive effect in semiconductors," in *Photorefractive Materials and Their Applications I,* P. Günter and J. P. Huignard, Eds., pp. 237–262, Springer-Verlag, Berlin (1988).
7. A. M. Glass, "The photorefractive effect," *Opt. Eng.* **17,** 470–479 (1978).
8. R. Magnusson, J. H. Mitchell III, T. D. Black, and D. R. Wilson, "Holographic interferometry using iron-doped lithium niobate," *Appl. Phys. Lett.* **51,** 81–82 (1987).
9. A. Hafiz, R. Magnusson, J. S. Bagby, D. R. Wilson, and T. D. Black, "Visualization of aerodynamic flow fields using photorefractive crystals," *Appl. Opt.* **28,** 1521–1524 (1989).
10. R. Magnusson, A. Hafiz, J. S. Bagby, and A. Haji-Sheikh, "Holographic interferometry using self-developing optical crystals for heat flux evaluation," *J. Electron. Packaging* **112,** 225–259 (1990).
11. H. Kogelnik, "Coupled wave theory for thick hologram gratings," *Bell Syst. Tech J.* **48,** 2909–2947 (1990).
12. D. von der Linde and A. M. Glass, "Photorefractive effects for reversible holographic storage of information," *Appl. Phys.* **8,** 85–100 (1975).
13. V. E. Wood, R. C. Sherman, N. F. Hartman, and C. M. Verber, "Optical erasure of one- and two-photon holograms in Fe-doped $LiNbO_3$," *Ferroelectrics* **34,** 175–178 (1981).
14. D. Gabor, G. W. Stroke, R. Restrick, A. Funkhouser, and D. Brumm, "Optical image synthesis (complex amplitude addition and subtraction) by holographic Fourier transformation," *Phys. Lett.* **18,** 116–118 (1965).
15. J. P. Huignard, J. P. Herriau, and F. Micheron, "Coherent selective erasure of superimposed volume holograms in $LiNbO_3$," *Appl. Phys. Lett.* **26,** 256–258 (1975).
16. J. D. Trolinger, "Application of generalized phase control during reconstruction to flow visualization holography," *Appl. Opt.* **18,** 766–774 (1979).
17. C. C. Guest, M. M. Mirsalehi, and T. K. Gaylord, "EXCLUSIVE OR processing (binary image subtraction) using thick Fourier holograms," *Appl. Opt.* **23,** 3444–3454 (1984).
18. P. Hariharan, *Optical Holography: Principles, Techniques and Applications,* Cambridge University Press, Cambridge (1984).
19. J. P. Huignard and J. P. Herriau, "Real-time double-exposure interferometry with $Bi_{12}SiO_{20}$ crystals in transverse electrooptic configuration," *Appl. Opt.* **16,** 1807–1809 (1977).
20. Y. H. Ja, "Real-time double-exposure holographic interferometry in four-wave mixing with photorefractive $Bi_{12}GeO_{20}$ crystals," *Appl. Opt.* **21,** 3230–3231 (1982).
21. X. Wang, R. Magnusson, and A. Haji-Sheikh, "Real-time interferometry with photorefractive reference holograms," *Appl. Opt.* **32,** 1983–1986 (1993).

Robert Magnusson received the MSEE and PhD degrees from the Georgia Institute of Technology in 1973 and 1976, respectively. He joined the faculty of the University of Texas at Arlington in 1984, where he established the Electro-Optics Research Laboratory. Currently he is a professor of electrical engineering with research interests including diffractive optics, integrated optics, holography, photorefraction, and optical filters. He is the author or coauthor of around 100 journal articles and conference papers. He is a member of SPIE, OSA, IEEE, Sigma Xi, and Tau Beta Pi.

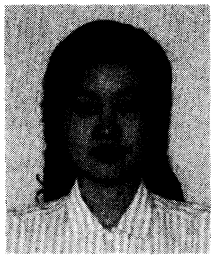

Xuqun Wang received the BS degree in optics from Shandong University, Jinan, China, in 1982 and the ME degree in optical engineering from Beijing Institute of Technology, China, in 1986. She also earned an MS degree in electrical engineering from the University of Texas at Arlington in 1990; she then served as a research engineer at the University of Texas at Arlington for two years. She is currently an engineer with Spectra Diode Labs in San Jose, California.

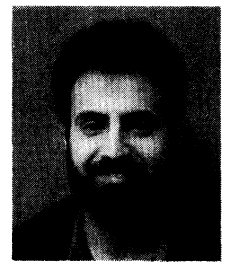

Ali Hafiz received the MS and PhD degrees in electrical engineering from the University of Texas at Arlington in 1989 and 1993, respectively. He is currently performing postdoctoral research at the same university. His research interests include holographic storage in photorefractive materials, holographic interferometry, picosecond and nanosecond holography in photorefractive materials, optoelectronics, and optical communications. He is a member of OSA, IEEE, Eta Kappa Nu, and Sigma Xi.

Truman D. Black received the BS degree in physics from the University of Houston in 1959, and MA and PhD degrees in physics from Rice University in 1961 and 1964, respectively. He was a member of the scientific and technical staff of Texas Instruments in Dallas for two years before joining the faculty of the University of Texas at Arlington in 1966 where he is a professor of physics. His research interests include acousto-optics, diffractive optics, holography, photorefractive materials, and microwave magnetic resonance in solids including superconductors. He is author or coauthor of more than 100 journal articles and conference papers. He is a member of APS, OSA, and Sigma Xi.

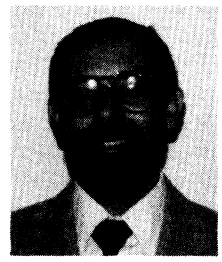

Lucio N. Tello received the BS degree in electronics from the Universidad Distrital, Bogota, Columbia, in 1975 and the MS and DSc degrees in physics from the University of Texas at Arlington in 1983 and 1992, respectively. His research interests include characterization of ultrasonic transducers by optical methods. He currently works for Computalog Research Inc. as senior research engineer. Dr. Tello is a member of the Society of Professional Well Log Analysts.

A. Haji-Sheikh received the MS degree in mechanical engineering and the MA degree in mathematics, both from the University of Michigan, Ann Arbor, and the PhD degree in mechanical engineering (heat transfer) from the University of Minnesota, Minneapolis/St. Paul. He is presently professor of mechanical engineering at the University of Texas at Arlington. He has authored nearly 100 papers in various journals and is author or coauthor of chapters in numerous books.

Snezana Konecni received the BS degree in mechanical engineering from Kiril and Metodij University, Skopje, Macedonia, Yugoslavia, in 1988, and the MS degree in mechanical engineering from the University of Texas at Arlington in 1990. She is currently a PhD candidate in the Mechanical and Aerospace Engineering Department at the University of Texas at Arlington. Her research interests include heat transfer from electronic equipment and holographic interferometry. She is a member of ASME, Tau Beta Pi, and Sigma Xi.

Donald R. Wilson received the BS degree in aerospace engineering from the Georgia Institute of Technology in 1961, the MS degree in aerospace engineering from the University of Tennessee in 1965, and the PhD degree in engineering from the University of Texas at Arlington (UTA) in 1973. Prior to joining the faculty of UTA, he was employed as a research project engineer at the Air Force Arnold Engineering Development Center, Tennessee, from 1962 to 1967, and as a lead propulsion engineer at the LTV Missiles and Space Company, Texas, from 1967 to 1968. He was responsible for the development of the Aerodynamics Research Center at UTA and served as its director from 1986 to 1992. He is currently director of the Aerospace Engineering Program at UTA. His technical interests include gas dynamics, high-speed aerodynamics, and aerospace propulsion.